npj | Flexible Electronics

www.nature.com/npjflexelectron

ARTICLE OPEN

Multiscale nanowire-microfluidic hybrid strain sensors with high sensitivity and stretchability

Songjia Han[1], Chunrui Liu[1], Huihua Xu[1], Dongyuan Yao[1], Kanghong Yan[1], Huanliang Zheng[1], Hui-Jiuan Chen[1], Xuchun Gui[1], Sheng Chu[2] and Chuan Liu[1]

Nanomaterials with low-dimensional morphology have been explored for enhancing the performance of strain sensors, but it remains difficult to achieve high stretchability and sensitivity simultaneously. In this work, a composite structure strain sensor based on nanomaterials and conductive liquid is designed, demonstrated, and engineered. The nanowire-microfluidic hybrid (NMH) strain sensor responds to multiscale strains from 4% to over 400%, with a high sensitivity and durability under small strain. Metal nanowires and carbon nanotubes are used to fabricate the NMH strain sensors, which simultaneously exhibit record-high average gauge factors and stretchability, far better than the conventional nanowire devices. Quantitative modeling of the electrical characteristics reveals that the effective conductivity percolation through the hybrid structures is the key to achieving high gauge factors for multiscale sensing. The sensors can operate at low voltages and are capable of responding to various mechanical deformations. When fixed on human skin, the sensors can monitor large-scale deformations (skeleton motion) and small-scale deformations (facial expressions and pulses). The sensors are also employed in multichannel, interactive electronic system for wireless control of robotics. Such demonstrations indicate the potential of the sensors as wearable detectors for human motion or as bionic ligaments in soft robotics.

npj Flexible Electronics (2018)2:16 ; doi:10.1038/s41528-018-0029-x

INTRODUCTION

In recent years, strain sensors have shown potential for soft electronics applications because they can be used for human body motion detection, human health monitoring systems, and man–machine interactions.[1,2] In addition, strain sensors can also be useful for building artificial body parts for humans, soft robotics, and bionic robotics in the future.[3] Strain sensors are classified as piezoresistive, piezoelectric, or piezocapacitive.[4–8] Piezoresistive strain sensors respond to mechanical signals with a change in the electrical resistance in the device due to a change in the length. Current piezoresistive strain sensors can monitor small human motions with small-scale deformations (<10%), such as facial expressions, pulse waves, and respiration. However, to construct artificial body parts or soft robotics in the future, multiscale strain sensors must be able to tolerate large-scale deformations (>70%) and detect stretching and contracting. High stretchability is an essential feature for newly developed strain sensors. In addition, other important characteristics, such as long-term stability and durability, rapid response, and low cost, are needed for practical wearable devices.[3,9]

Low-dimensional nanomaterials have greatly advanced strain sensor research, and they outperform traditional semiconductors or metal foils that only work when the strain (ε) is below 5%,[3,10] as the materials are brittle and allow only small strains. Various studies have focused on using nanomaterials to improve sensor performance, including carbon nanotubes (CNTs),[11,12] silver nanowires (AgNWs),[6] copper nanowires (CuNWs),[13] gold nanowires (AuNWs),[14,15] graphene nanosheets,[16,17] graphene foam,[18] carbon-black particles,[19,20] silver nanoparticles (AgNPs), and their composite materials.[21] Nanomaterials are commonly embedded into elastic polymers to form conductive networks,[22] and the device resistance increases as the area/volume fraction decreases under mechanical stimulation. For example, Amjadi et al. fabricated strain sensors based on a AgNW/PDMS composite with a stretchability of ~70%.[23] Roh et al. created CNT-based sensors that can be stretched to 100% before failure.[7] To improve the sensitivity of strain sensor, structural crack formation is an effective way to induce the change of resistance. Wang and coauthors printed AgNP on a polyurethane acrylate substrate to fabricate a structure-dependent device. The gauge factor (GF) of the strain sensor is as high as 10^7 at strain of 12%.[24] Kim's group fabricated a high-sensitivity crack-based sensor by controlling crack depth. The device exhibited an ultrahigh GF ≈ 16,000 at 2% strain.[25] Zhu et al. investigated the effect of cut-through channel cracks on improving the sensitivity of strain sensor. The developed strain sensor performed a high GF greater than 5000 under the strain of 1%.[26] However, the sensor with a high sensitivity cannot maintain an intact conductive network when they are stretched under a large-scale strain (e.g., over 200%)[27] because the conductive nanomaterial volume fraction decreases to below the electrical conduction percolation threshold, and the strain sensor loses its conductivity.

Other methods to create strain sensors with improved stretchability have been proposed, such as pre-stretching, 3D-printing, microfluidic, and wave-fabric design techniques.[28–32] For

[1]State Key Laboratory of Optoelectronic Materials and Technologies and the Guangdong Province Key Laboratory of Display Material and Technology, School of Electronics and Information Technology, Sun Yat-Sen University, Guangzhou 510275, China and [2]State Key Laboratory for Optoelectronics Materials and Technology, School of Materials Science and Engineering Sun Yat-Sen University, Guangzhou 510275, China
Correspondence: Chuan Liu (liuchuan5@mail.sysu.edu.cn)

Received: 4 January 2018 Revised: 17 April 2018 Accepted: 20 April 2018
Published online: 04 June 2018

example, Muth et al. used embedded, 3D printing to fabricate strain sensors with conductive carbon grease materials to obtain a high stretchability of 400%.[32] However, simultaneously obtaining a high endurance with a large-scale deformation and a high sensitivity under a small-scale strain is a challenge for nanowire-based sensors,[33] and these properties are scientifically interesting and suitable for joints or units in soft robotics with multiscale movements.[34] In general, a low volume fraction of conductive nanomaterials results in high sensitivity but relatively low stretchability, whereas a high fraction of conductive nanomaterials results in higher stretchability but lower sensitivity. Ideally, a single sensing device would have a large stretchability as well as a high GF, which measures the change in the electrical resistance upon deformation.

We present a new strategy to create nanowire-based strain sensors by hybridizing brittle metal nanowires (AgNWs, CuNWs, or CNTs) and a conductive organic solution, poly(3,4-ethylenedioxythiophene):polystyrene sulfonate (PEDOT:PSS). The nanowire-microfluidic hybrid (NMH) strain sensors exhibit record-high values for both the GF and stretchability. This is because the advantages of the two materials have been coupled. The brittleness of the nanowires endows the strain sensor with an outstanding sensitivity under a small stretchable load, and the conductive organic solution significantly enhances the deformation endurance of the device. Quantitative investigations show that the conductive solution provides an electrical percolation path when the nanowires disconnect under a large strain to provide multiscale sensing. Various demonstrations have been performed to detect tiny mechanical deformations, e.g., pulses or facial expressions, and monitor larger stretchable deformations, such as human joint movements. The present study offers a new type of sensor that will be especially useful for multiscale sensing and potentially suitable for artificial joints or sensing units in soft robotics.

RESULTS AND DISCUSSION

Electrical characterizations

Figure 1 illustrates the procedure for fabricating the strain sensor mainly based on the solution process: (1) polyimide (PI) tape is attached to a glass substrate to create microchannels. (2) A nanowire suspension solution is deposited on the PI tape to form conductive thin films. (3) The Ecoflex prepolymer is spin-coated onto the film and cured. (4) The Ecoflex film is peeled off the substrate to form microchannels. (5) Silver wires are connected at both ends of the microchannels to form contacts, and then, another Ecoflex slab is used to cover the device. (6) The PEDOT:PSS solution is injected into the microchannels using a syringe. Then, a NMH strain sensor with a conductive nanowire network and a conductive solution is created.

To examine the advantages of the proposed structure, four types of structures were fabricated: (I) a pure CuNW film (measured resistance of 26 Ω); (II) a pure PEDOT:PSS solution (5000 Ω); (III) a CuNW film combined with a solid-state PEDOT:PSS film (29.4 Ω); and (IV) a CuNW film combined with the liquid-state PEDOT:PSS solution (26.4 Ω). The current−voltage curves of these strain sensors are shown in Fig. 2a. Because the initial resistance of

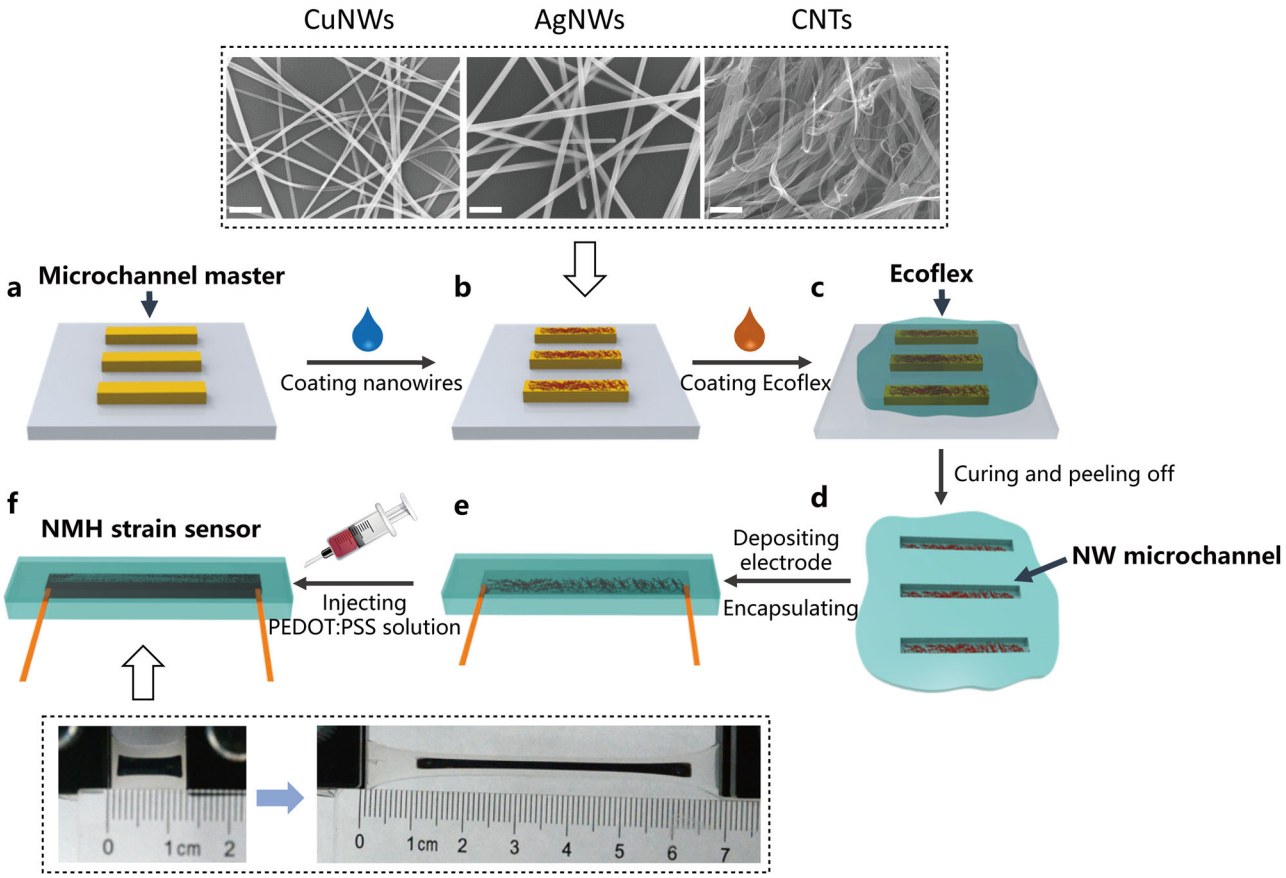

Fig. 1 Schematic diagram of the fabrication process for the nanowire-microfluidic hybrid (NMH) strain sensor. **a** Attach PI tape to a glass substrate. **b** Deposit nanowires or nanotubes onto the PI tape to form conductive thin films. Scanning electron microscopy (SEM) images of the synthesized copper, silver nanowires, or carbon nanotubes are shown above (the scale bars represent 400 nm). **c** Pour and impregnate the conductive thin film with uncured Ecoflex. **d** Peel off the Ecoflex film after curing. **e** Attach silver wires and encapsulate. **f** Inject the PEDOT:PSS solution and seal the channel with Ecoflex. Photos of the obtained NMH sensors under different scales of stretching are also shown

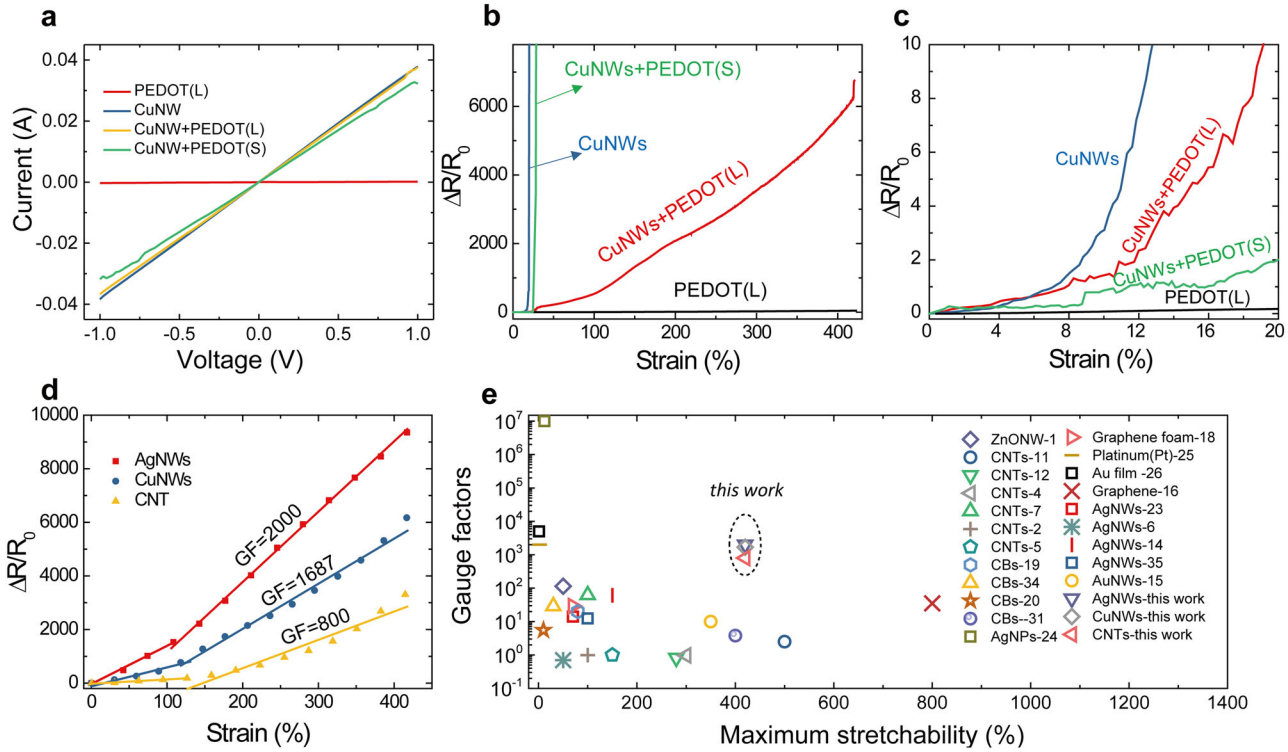

Fig. 2 Electromechanical properties of the strain sensors. **a** *I–V* curves of the strain sensors with different structures; PEDOT denotes PEDOT:PSS. **b** Relative resistance variations of the sensors during stretching. **c** Relative resistance variations of the sensors under a small strain. **d** Relative changes in the resistances of the sensors based on AgNWs, CuNWs, or carbon nanotubes (CNTs) from 0 to 420% strain. Extraction of the GFs by linearly fitting the plot of the electrical resistance variation as a function of the applied strain. **e** Comparisons of the average GFs against the maximum stretchability for previously reported strain sensors

the CuNW film is far lower than the resistance of the PEDOT:PSS solution, the primary resistance of the hybrid structural strain sensor is mainly dominated by the property of the nanowire film. These strain sensors were tested under strains, and the electrical responses were characterized by the variations in the relative resistances, $\Delta R/R_0 = (R–R_0)/R_0$, where R_0 and R correspond to the original resistance and the real-time resistance under stretching, respectively. Figure 2b shows the values of $\Delta R/R_0$ with respect to the strain, $\varepsilon = (L–L_0)/L_0$, where L_0 and L correspond to the original length and stretching length, respectively.[35,36] The strain sensor based on the pure CuNW film showed the lowest stretchability. The sample was damaged at $\sim\varepsilon = 19\%$, and its resistance immediately increased to a high value. When multiple layers were introduced to improve the strain sensor stretchability,[7,37] the sensors with the CuNW film coated with a solid-state PEDOT:PSS film performed well until mechanical failure at $\varepsilon = 25\%$. The limited stretchability is due to the poor adhesion between the CuNW and PEDOT:PSS films. In contrast, the sensor with the CuNW film and PEDOT:PSS solution performed well, even when it was stretched up to 420% of its original length. This is comparable to the performance of a traditional microfluidic strain sensor with a pure PEDOT:PSS solution, but the combination sensor has a much higher sensitivity for large variations in the relative resistances. Figure 2c shows the $\Delta R/R_0$ values at small strains. The sensitivity is quantified by calculating a figure of merit, i.e., the GF, which is defined as $GF = (dR/R_0)/(dL/L_0)$. Here, R_0 and L_0 are the original resistance and length of the sensor, and dR and dL are the changes in the resistance and length of the sensor under loading.[32] The GF of the CuNW/PEDOT:PSS(L) strain sensor is obtained by fitting the relative change in the resistance–strain curve, as shown in Fig. 2d. The GF is about 8 under 6% strain, 10 under 10% strain, and 30 under 16% strain, and when strain increased to 420%, the GF is as high as 1678.

In addition to CuNWs, other nanomaterials, e.g., AgNWs or CNT with PEDOT(L), were also employed to fabricate sensors, and the $\Delta R/R_0$ values are shown in Fig. 2d. The results show that the NMH structure can be broadly used to improve the properties of strain sensors based on nanowires. The trends in the evolution of the $\Delta R/R_0$ values for these strain sensors are different. The AgNW sensor has the fastest change in the $\Delta R/R_0$ values due to its low original resistance (11 Ω), while the CNT sensor has a slower change in the $\Delta R/R_0$ values because of its relatively high original resistance (51 Ω). To investigate the effect of concentration of NWs or CNTs on sensor performance, we fabricated a series of CNT-based sensors with different initial resistances. As shown in Figure S1, we find that all sensors show a large working range from the strain of 0 to ~420%. The larger the initial resistance of the CNT films, the smaller the relative resistance variations. It indicates that the sensitivity of the sensor can be adjusted by the concentration of NWs or CNTs.

The average GFs against the maximum stretchability of the presented sensors are compared with those of recently reported strain sensors, as shown in Fig. 2e. Most traditional strain sensors have a high GF but only work under a small strain range, or they exhibit a low GF value and work over a broad sensing range. The trade-off between a “large stretchability” and a “high sensitivity” is attributed to the limitations of the mechanical and electrical characteristics of a single material. In comparison, the presented hybrid strain sensors have high GFs under a large strain range. Especially, the devices created with AgNWs or CuNWs have very high GF values of 2000 and 1678, respectively. The GF of a CNT-based device is lower, ~800, which is still higher than that of most traditional sensors. Hence, the hybrid strain sensors exhibit improved stretchability and sensitivity compared with other reported structures and are suitable for multiscale sensing.

Strain cycling tests, including a loading and unloading cycle (strain from 0 to 420 to 0%), were performed, as shown in Figure S2 in Supplementary information (SI). The devices have normal electrical responses under the full-scale strain stretching and exhibit some hysteresis in the stretching–relaxing cycles. Nevertheless, the sensor generally presents a good reproducibility over 3000 cycles, as shown in Figure S3.

In addition to stretchability and sensitivity, strain sensors must have a fast response speed and different reactions to various mechanical stimulations, e.g., tension, compression, and pressure. Figure 3a presents the $\Delta R/R_0$ values of the strain sensor when it was stretched to a small-scale strain with a test frequency of 0.5 Hz. In this test, the strain sensor responds well to a change as small as $\varepsilon = 4\%$, which indicates that the sensor can be used to

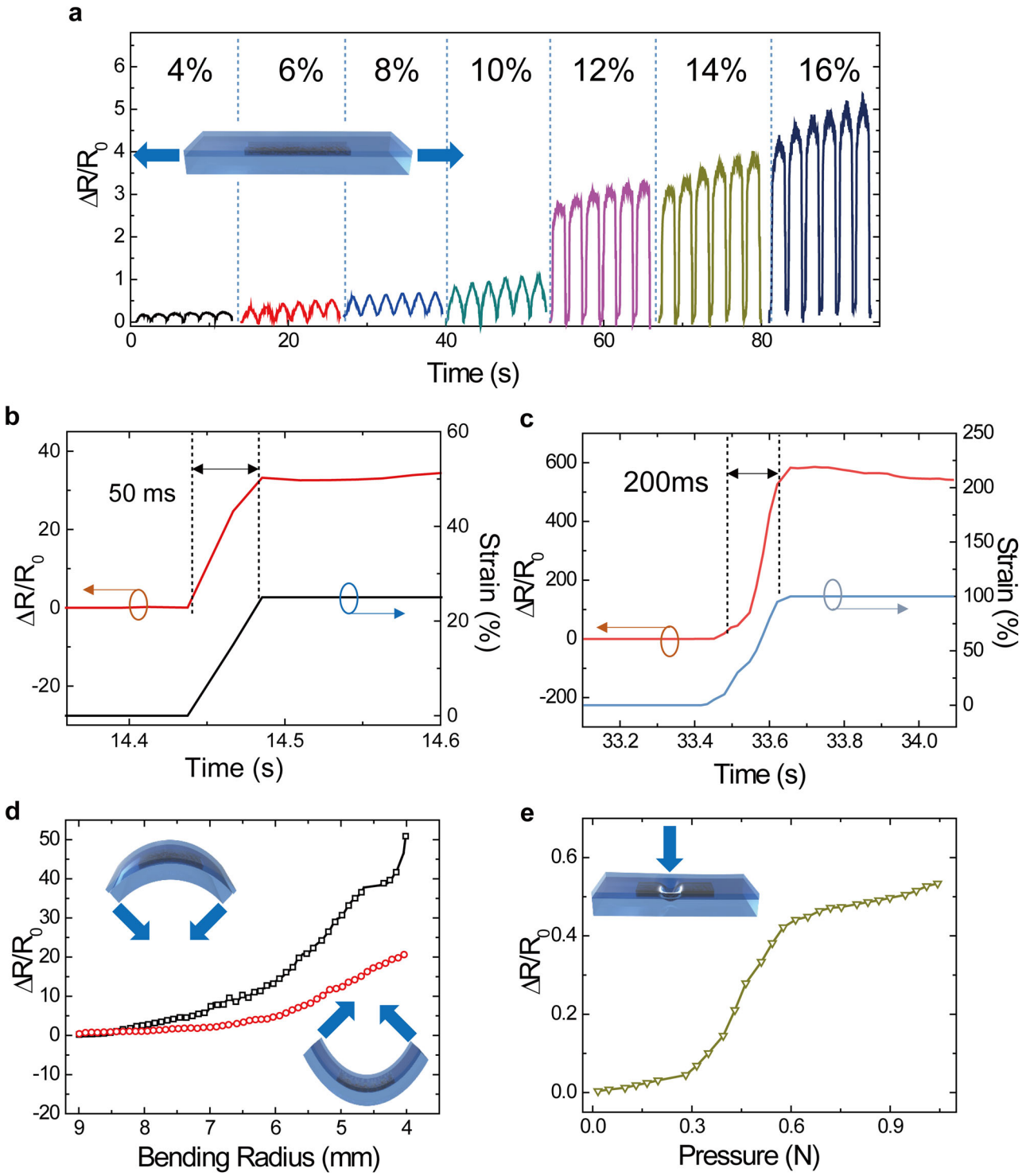

Fig. 3 Relative changes in the sensor resistance under various dynamic loadings: **a** Relative change in the resistance under different strains. **b** Instant response to small stretching, i.e., the resistance of the strain sensor (blue) for 0–25% strain (red). **c** Instant response to large stretching, i.e., the resistance of the strain sensor (blue) for 0–100% strain (red). **d** Relative change in the resistance for a bending radius of 5−9 mm with tension (black line) or compression (red line). **e** Relative change in the resistance of the NMH strain sensor under pressure (0–1 N)

detect tiny deformations. Figure 3b, c shows the instant responses for the resistance sensor under a small-scale strain ($\varepsilon = 25\%$) and a large-scale strain ($\varepsilon = 100\%$), respectively. The sensor has a rapid mechanical response, and the $\Delta R/R_0$ values increase within 50 ms when the strain is <25%. When the sensor is subjected to quick stretching under a large-scale strain ($\varepsilon = 100\%$), it quickly responds with the $\Delta R/R_0$ values at ~200 ms. The $\Delta R/R_0$ values of the strain sensor were measured under different mechanical actions, as shown in Fig. 3d, e. First, the sensor was subjected to tension bending with radii from 9 to 5 mm (Fig. 3d, black). The $\Delta R/R_0$ values increase when the bending radius decreases, which is caused by the stretching of the CuNW film and a reduction in the cross-section of the PEDOT:PSS solution. Second, the sensor was subjected to compression with radii from 9 to 5 mm (Fig. 3d, red), and the $\Delta R/R_0$ values increase up to 50 as the radius decreases. Compression may cause the CuNWs wrinkled and overlapped and would reduce the conductive path of a conductive network, thus increasing the resistance. Third, the sensor was subjected to a pressure test, as shown in Fig. 3e. When subjected to a constant force, the conductive network is prone to deformation because of its cavities, and the $\Delta R/R_0$ values gradually increase. The above tests show that the presented sensor possesses the desirable features of high sensitivity, wide sensing range, fast response, and multiple mechanical reactions.

Working mechanisms

The working mechanism of the sensor was first investigated by tracking the microstructural evolution and crack propagation of the CuNW/Ecoflex film during stretching. Before the stretching, the surface of the CuNW film is smooth, and the conductive network is integrated, as shown in the SEM image (Fig. 4a). When the film is stretched, the CuNWs begin to break and slide from the matrix, as shown in Fig. 4b. Several cracks appear on the surface of the CuNW film, indicating damage in the conductive network. With increasing deformation, the cracks grow, and the conductive network is eventually destroyed, as shown in Fig. 4c. The high-resolution SEM image of the film fragment edge shows that some CuNWs are removed from the matrix and cannot return to their initial positions after the stress is released. As a result, the electrical resistance of the nanowire network is expected to sharply increase, which is similar to the results in previously reported work.[38–40]

The resistance of the presented sensor does not follow that of the pure nanowire network and gradually increases under a large-scale strain. The working principle is explained by the electric percolation between the parallel nanowire network and the microfluidic channels, as schematically illustrated in Fig. 4d–f. In general, the working mechanisms can be divided into three regimes. (i) Initially, the resistance of the nanowire film, R_N, is much smaller than the resistance of the conductive liquid PEDOT:PSS solution (R_M), and the current mainly passes through the nanowire network. Then, the resistance, R, exponentially increases with the distance, d, between the nanowires and nanotubes.[41] (ii) When the sensor is under a small-scale strain, the slippage and fracture of the nanowires in the elastic matrix decrease the contact area between the nanowires and increase the resistance of the nanowire network (Fig. 4e). However, due to the PEDOT:PSS solution, a percolation path forms through the solid–liquid hybrid, which can maintain the integrity of the conductive network and prevent the conductive pathways from breaking under a large deformation. The overall resistance depends on the parallel resistance of the nanowire film and PEDOT:PSS solution. (iii) When the strain amplitude increases and the sensor is under a large-scale strain, the large number of cracks in the nanowire network become large gaps (Fig. 4f), leading to a remarkable increase in the resistance of the nanowire film. Then, the conductive PEDOT:

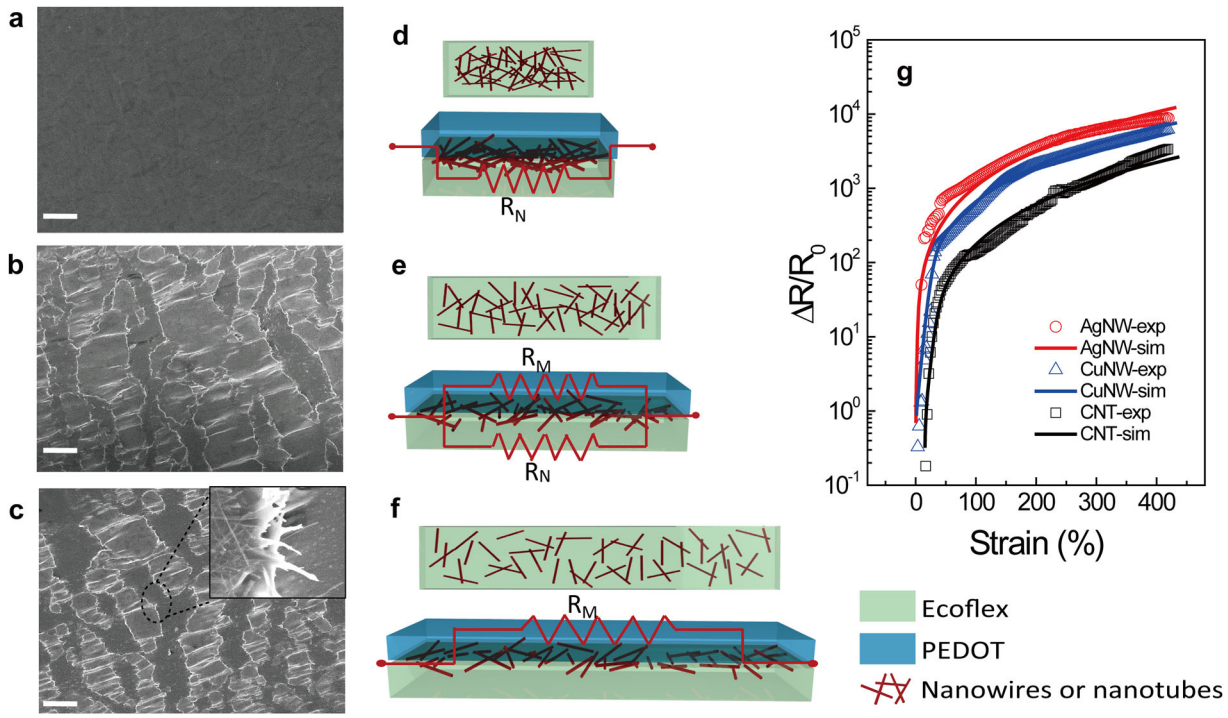

Fig. 4 SEM images of the CuNW/Ecoflex composite under different strains: **a** 0%, **b** 15%, and **c** 80% (the inset is the magnified crack). The scale bar is 60 μm. **c**, **f** Corresponding schematic diagrams of stretched nanowire or nanotube networks (upper) and stretched devices (lower), showing the resistance networks. These schemes illustrate the conducting mechanisms of the NMH strain sensors corresponding to the evolution of the morphology on the left. **g** Relative change in the resistance of the NMH strain sensor obtained from experiments (open dots) and simulations using the proposed percolation model (curves)

PSS solution provides the only continuous conductive path for electrical sensing.[42]

Accordingly, the variance in the resistance of the sensor, D, can be calculated by the following equations:

$$R_N = R_{N0}\left[\frac{d}{d_0}\exp(A_1(d-d_0)) - 1\right] \quad (1)$$

$$R_M = R_{M0}(\varepsilon+1)^2\left(\frac{\varepsilon}{1+\varepsilon}\right) = R_{M0}\varepsilon(\varepsilon+1) \quad (2)$$

$$R = \frac{R_N \cdot R_M}{R_N + R_M} \quad (3)$$

$$D = \frac{\Delta R}{R} = \frac{R - R_{N0}}{R_{N0}} \quad (4)$$

$$D = \frac{\varepsilon\cdot(\varepsilon+1)\cdot[(1+\varepsilon)\cdot\exp(A_1\cdot d_0\cdot\varepsilon) - 1]}{\frac{R_{N0}}{R_{M0}}\cdot[(1+\varepsilon)\cdot\exp(A_1\cdot d_0\cdot\varepsilon) - 1] + \varepsilon\cdot(\varepsilon+1)} - 1 \quad (5)$$

where ε is the applied strain, as stated above;[28] R_{N0} and R_{M0} are the initial resistances of the nanowire or nanotube film and the microfluidic channel, respectively; $\frac{\varepsilon}{1+\varepsilon}$ represents the portion of the solution filling up the gap in the nanowire or nanotube film; and d_0 is the average distance for electron tunneling at rest and is approximately $d=d_0(\varepsilon+1)$. The proposed equations were used to simulate the variance in the resistance of the sensor D, and according to Equation (5), we find that the resistance variation of the sensor under a certain strain is mainly affected by the ratio of R_{N0} and R_{M0}, which may be related to the thickness of the nanowire solid film as well as the liquid microchannel in the device. The theoretic data are compared to the experimental data, as shown in Fig. 4g (see more details in the SI). While the model is simple, a reasonable agreement between the theoretical simulations and experimental results was obtained for the different strain sensors. The deviations are probably caused by the contact resistance between the nanowires or nanotubes and the conductive solutions, as well as the contact resistance at the electrodes. Nevertheless, the above model explains the working principle of the hybrid sensor at various sensing scales.

Sensing demonstrations

Human body deformations can be roughly divided into three regimes, as shown in Fig. 5a, i.e., small-scale (<5%); middle-scale (5–50%), and large-scale (50–100%). When the strain is beyond

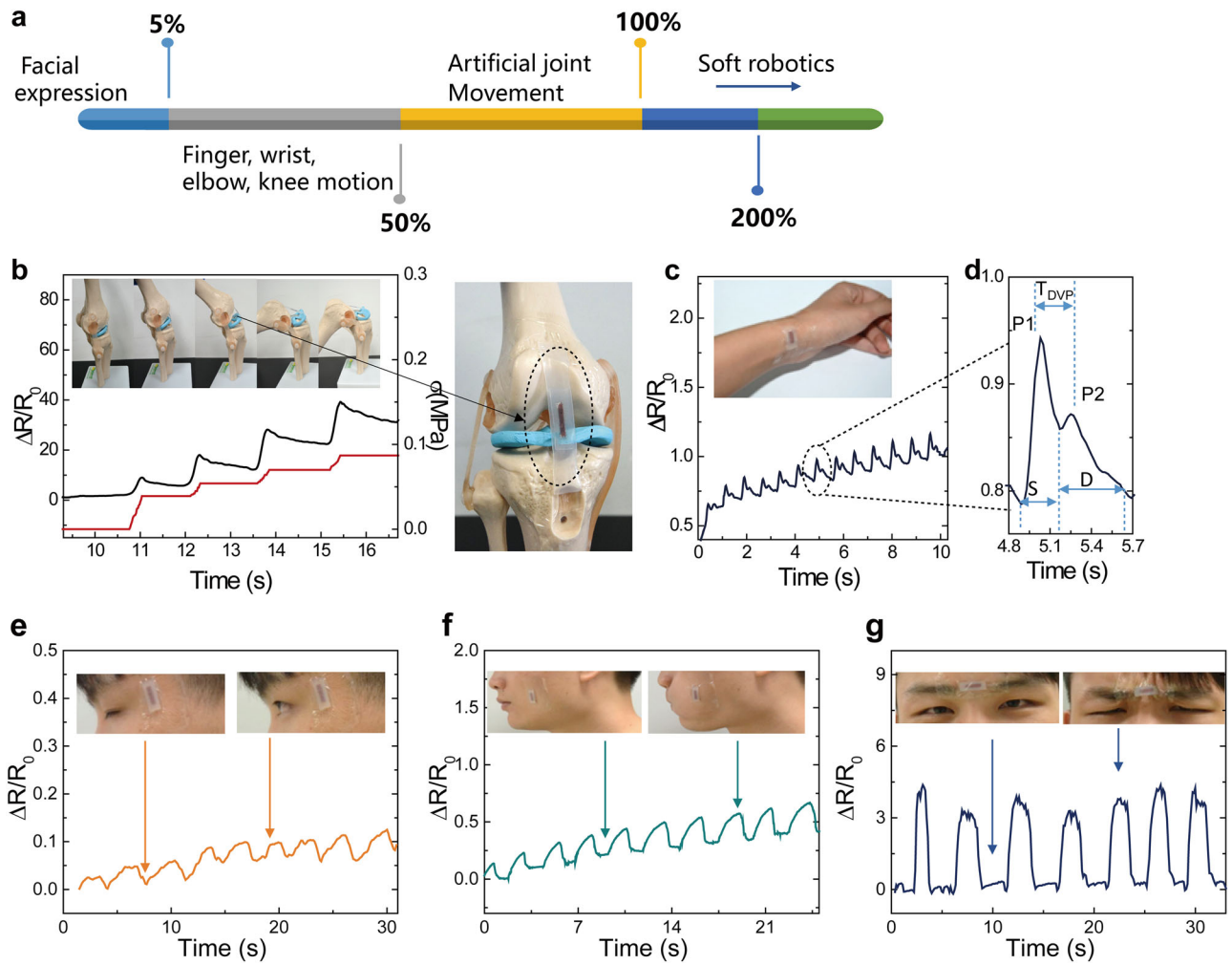

Fig. 5 **a** Illustration of the human activity and the approximate range of strain scales. **b** Relative resistance responses of the NMH strain sensor for detecting the bending state of a skeleton knee model (black), and the tensile strength of the NMH strain sensor under different deformations (red). **c**–**g** Detection of small-scale human body deformations by the NMH strain sensor: **c** Relative change in the resistance of the sensor monitoring the pulse on a human wrist. (**d**) A typical pulse waveform is shown on the right. **e** Eye blinking, **f** cheek movement, and **g** frown

100%, the regime can be used for soft robotics. In the subsequent discussion, the hybrid sensor is used for multiscale sensing to monitor the human body. Figure 5b shows the sensor mounted on a knee skeleton model to simulate ligament movement. When the skeleton model was bent to imitate human knee activity, both the resistance variation and tensile strength of the sensor gradually increase as the bending angle increases. The sensor was mounted onto human skin to monitor slight human activity, such as pulse and facial expressions. In addition to the significant changes in the sensor resistance, it is also important that the sensor can deform even with a small amount of tension. According to Hooke's law: $\varepsilon = \frac{\sigma}{E} = \frac{F}{S \cdot E}$, where ε is the applied strain, F is tension, E is Young's modulus of the substrate, and S is the cross-sectional area of sensor which depends on the thickness and width of the device. The Young's modulus of Ecoflex is as low as 0.15 MPa to allow sensitive reaction to strain. Also, notice that the cross-sectional area of the NMH sensor is smaller than a conventional bulk device due to the existence of a microchannel. Hence, our device is able to reflect and monitor human tiny activity. As shown in Fig. 5c, a sensor was attached to the skin over the artery in a human wrist to record the pulse signal. A periodic pulse wave of 13 peaks in 10 s is observed, and the signal waves are regular and repeatable. Figure 5d shows the waveforms, which reflect the systolic and diastolic ventricle activity. The systolic ventricular period is ~0.3 s, and the diastolic period is ~0.5 s. The transit time (ΔT_{DVP}) is 0.27 s. Note that the base signals of resistance slightly increase with cycling due to the buckling of the nanowire-based structure. When the sensor was stretched, strain in the nanowires was much smaller than the applied strain to the substrate, and thus the nanowires would slightly slide on the substrate. However, after releasing strain, the nanowire would not slide back to the initial position and form a nanowire buckle under compression. Thus, the resistance would not fully restore to the initial level as the conductive paths of the network were reduced by the nanowire buckles.[43,44] Furthermore, a smaller-scale sensing is further shown by monitoring facial expressions, which express the human emotional state by referring to changes in internal muscles in the eyes, face, and mouth. Figure 5e, f shows the signals for a device mounted on a human canthus and cheek. When the eyes blink or the cheek moves, the device can detect small facial muscle movements by exhibiting an increased resistance. Interestingly, the sensor is also sensitive enough to monitor a frown (Fig. 5g).

In order to monitoring middle-scale deformation, the sensor was mounted on an elbow (see insets of Fig. 6a) or wrist (Fig. 6b) to record the bending process. In the bending cycles, the NMH strain sensor shows a rapid response and favorable reproducibility. Furthermore, the sensor can also be used to discriminate human body posture. Figure 6c shows the resistance change in a sensor integrated on the finger knuckles. The resistance variation increases in a stepwise manner in real time as the bending angle of the finger increases. In addition, the finger position, i.e., open and closed, can also be detected by mounting the sensor unit between the fingers (Fig. 6e). In addition, for a fast response and high sensitivity, the device can also be placed on a knee joint to detect and discriminate the motions of a human leg, such as walking, running, and squatting (Fig. 6d), based on the frequency and amplitude of the movement. When monitoring human activity, the noise level was about 20–60 nA. The noises may be caused by the surface type of detected item and shift in external temperature, which can be further reduced by forming intimate, conformal contact with the surface of the skin or by using a Wheatstone bridge configuration in our future work.[45,46]

The NMH sensors were integrated into a wireless-controlled, interactive electronic system. As shown in Fig. 6f, five NMH sensors were mounted on a thin glove and connected with a single-board microcontroller (Arduino UNO REV3). The finger motion data captured by the sensors were transferred by a Bluetooth kit to a robotic hand, controlling the opening and closing of each of the mechanical fingers. As shown in Fig. 6g–n and the Supplementary video (SI), multichannel sensing and dynamic controlling were successfully demonstrated, indicating good feasibility of the NMH sensors in human–robot interactive systems.

CONCLUSION

In summary, we proposed and fabricated NMH strain sensors that could be suitable for multiscale sensing. The device includes microchannels filled with a PEDOT:PSS solution and a conductive nanowire network embedded at the bottom of the microchannel. The hybrid structure provides a percolation path for electrical conduction, endowing the sensor with excellent sensitivity for small-scale strain and vast stretchability for large-scale strain. The hybrid structure is applicable for sensors based on nanomaterials, such as AgNWs, CuNWs, and CNTs, which exhibit brilliant deformation responses over a broad range of strain strengths. In addition, to prolong the lifetime of the sensor, the conductive PEDOT:PSS solution can be replaced by other conductive ionic liquids, such as ethylene glycol and glycerol, which have high boiling points and would afford longer lifetimes. The sensor can also indicate tension, compression, and pressure stimuli. The sensor works with low voltage and is comfortable to be worn on the human skin or attached to clothing for monitoring facial expressions, pulse, body motion, and gestures. This hybrid structure strain sensor may advance the realization of future soft electronic devices, such as smart robotics, electronic skin, human motion and health-monitoring systems, and human–machine interactive systems.

EXPERIMENTAL METHODS

Synthesis and fabrication of the conductive nanowire ink

CuNW ink:CuNWs were synthesized by a previously reported hydrothermal method.[47] Typically, 0.42 g of copper(II) chloride dehydrate ($CuCl_2{\cdot}2H_2O$) (99.999%, Sigma), 1 g of glucose (99.5%, Sigma), and 3.6 g of hexadecylamine (HDA) (98%, sigma) were added into a beaker with 200 mL of deionized water and stirred for 12 h to form an emulsion. $CuCl_2{\cdot}2H_2O$ is a precursor, glucose is a reductant, and HDA is the capping agent. Then, the resultant solution was transferred into a Teflon-lined autoclave to react at 110 °C for 6 h which forms a dark red-brown solution. The product was flushed with hexane and isopropanol (IPA). Finally, the obtained CuNWs were stored in an IPA solution. For the CNT ink, 0.1 g of CNTs (TNST, Timesnano) and 0.01 g of sodium dodecyl benzene sulfonic acid (SDBS) were added into a beaker with 100 mL of deionized water. Then, the admixture was homogeneously dispersed using an ultrasonic liquid processor (Qsonica, Q700) for 2 h to create the CNT ink. For the AgNWs, the AgNW ink was purchased from Kechuang Inc. and shaken for 10 min to form a suspension.

Coating the conductive nanowire films

Before fabricating the NW film, polyimide (PI) tape (width of 3 mm) was cut into 15-mm long strips and attached on a glass substrate to mark the microchannels. For the CuNW, AgNW, and CNT films, the corresponding ink was dropped onto the PI tape which formed a uniform network pattern due to surface tension. Then, the samples were annealed in a glove box at 350 °C for 20 min to remove the HDA absorbed on the surface and then, the samples were transferred. For the CNT film, the CNT ink was dropped onto the PI tape several times to form a conductive CNT network.

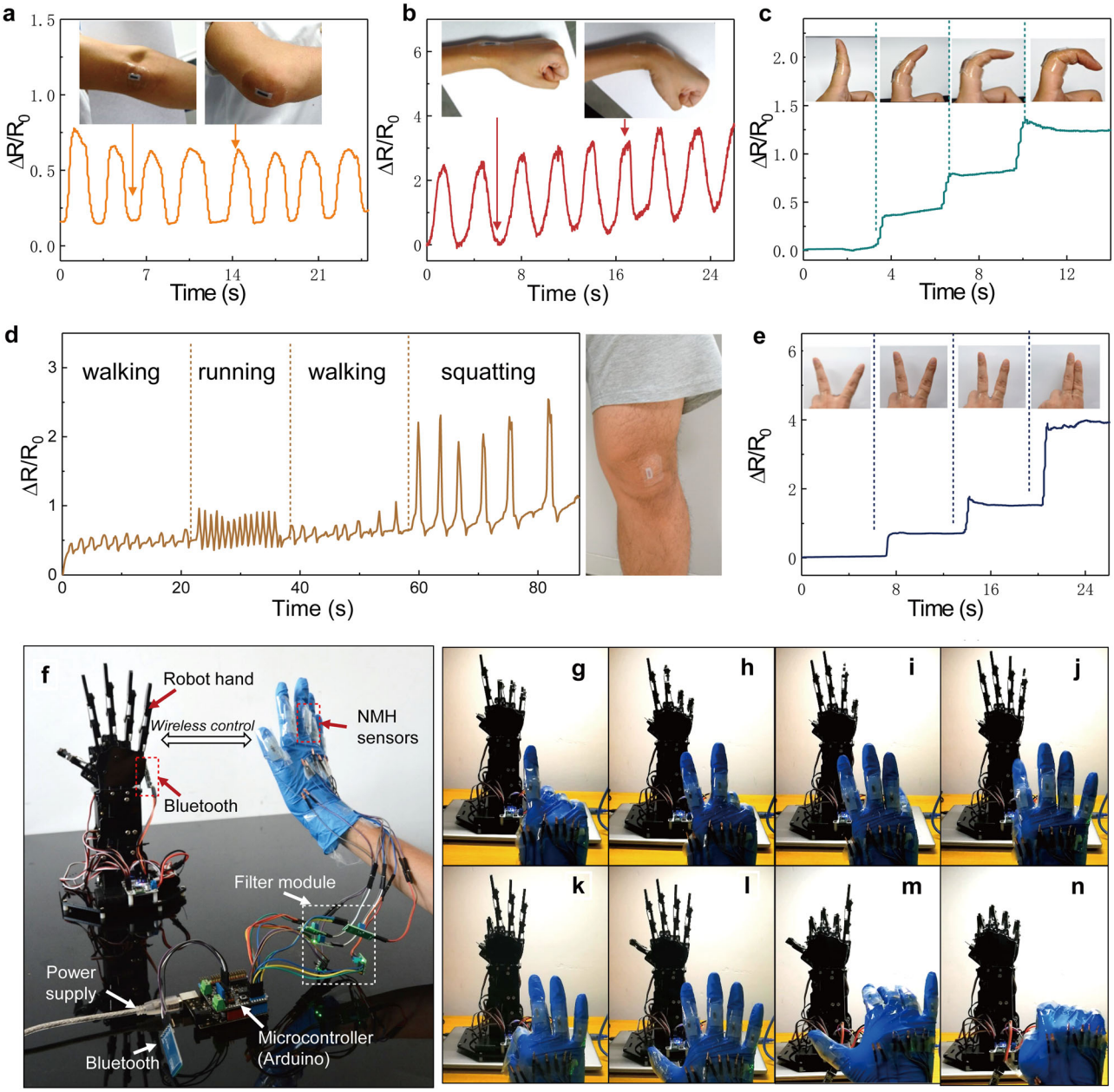

Fig. 6 Using the NMH strain sensor for human motion detection. **a–e** The relative change in the resistance of our strain sensor mounted on different locations of the human body: **a** elbow and **b** wrist bending. **c** Bending process of a finger. **d** Walking, running, and squatting of a knee joint. **e** Closing process of the fingers. **f** An interactive electronic system using a multichannel data-glove with five NMH sensors to control a robotic hand by wireless communication. **g–n** Control of different numbers of fingers of the robotic hand by a human hand wearing the data-glove with NMH sensors

Fabrication of the strain sensors

The hybrid strain sensor was fabricated via the following procedure. First, the stirred and degassed Ecoflex (ECOFLEX 0050, Smooth-On) was spin-coated on the annealed CuNW pattern and cured at room temperature for 2 h. Then, the Ecoflex film was peeled off the glass substrate to form the microchannels. Next, silver wires were attached to the ends of the embedded nanowires with a silver paste for further mechanical and electrical tests. Finally, a PEDOT:PSS solution (1.3–1.7 wt%, 4083 from Heraeus) was injected into the microchannels by a syringe, and the microchannels were sealed using another Ecoflex slab.

Electrical characterizations

Mechanical tests were carried out via a motorized moving stage (Zolix, SC300-3a), which can provide uniform stretching and releasing cycles. A cyclic press force was applied by a vibration exciter (Nanjing Buddha Science and Technology Co., HEV-20). To demonstrate the ability for real-time monitoring of human body motions, the sensors were mounted on the forefinger, finger web, wrist, elbow, or radial artery with Tegaderm Film (1624 W, 3 M). The resistance change in the strain sensors under the various deformations was measured by a Keithley 2400 Sourcemeter.

Data availability

The data sets generated during and/or analyzed during the current study are available from the corresponding author on reasonable request.

ACKNOWLEDGEMENTS

The authors gratefully acknowledge the financial support of the Guangdong Natural Science Funds for Distinguished Young Scholars under Grant 2016A030306046, the Guangdong Youth Top-notch Talent Support Program (No. 2016TQ03X648), and the "985" Project (30000-31101200).

AUTHOR CONTRIBUTIONS

S.H. performed the device design and fabrication. S.H. and C.L. performed the measurements. D.Y., K.Y., and H.Z. fabricated the multichannel-interactive electronic system. S.H. wrote the manuscript which was further improved by H.X., H.-J.C., X.G., and S.C. and then equally optimized by coauthors. C.L. supervised and coordinated the study. All authors have given approval of the final submission.

ADDITIONAL INFORMATION

Supplementary information accompanies the paper on the *npj Flexible Electronics* website (https://doi.org/10.1038/s41528-018-0029-x).

Competing interests: The authors declare no competing interests.

Publisher's note: Springer Nature remains neutral with regard to jurisdictional claims in published maps and institutional affiliations.

REFERENCES

1. Xiao, X. et al. High-strain sensors based on ZnO nanowire/polystyrene hybridized flexible films. *Adv. Mater.* **23**, 5440–5444 (2011).
2. Cohen, D. J., Mitra, D., Peterson, K. & Maharbiz, M. M. A highly elastic, capacitive strain gauge based on percolating nanotube networks. *Nano Lett.* **12**, 1821–1825 (2012).
3. Amjadi, M., Kyung, K.-U., Park, I. & Sitti, M. Stretchable, skin-mountable, and wearable strain sensors and their potential applications: a review. *Adv. Funct. Mater.* **26**, 1678–1698 (2016).
4. Cai, L. et al. Super-stretchable, transparent carbon nanotube-based capacitive strain sensors for human motion detection. *Sci. Rep.* **3**, 3048 (2013).
5. Shin, U.-H. et al. Highly stretchable conductors and piezocapacitive strain gauges based on simple contact-transfer patterning of carbon nanotube forests. *Carbon* **80**, 396–404 (2014).
6. Yao, S. & Zhu, Y. Wearable multifunctional sensors using printed stretchable conductors made of silver nanowires. *Nanoscale* **6**, 2345–2352 (2014).
7. Roh, E., Hwang, B. U., Kim, D., Kim, B. Y. & Lee, A. N. E. Stretchable, transparent, ultrasensitive, and patchable strain sensor for human-machine interfaces comprising a nanohybrid of carbon nanotubes and conductive elastomers. *ACS Nano* **9**, 9 (2015).
8. Yi, F. et al. Stretchable-rubber-based triboelectric nanogenerator and its application as self-powered body motion sensors. *Adv. Funct. Mater.* **25**, 3688–3696 (2015).
9. Liu, Z. et al. Thickness-gradient films for high gauge factor stretchable strain sensors. *Adv. Mater.* **27**, 6230–6237 (2015).
10. Zhou, J. et al. Flexible piezotronic strain sensor. *Nano Lett.* **8**, 5 (2008).
11. Amjadi, M., Yoon, Y. J. & Park, I. Ultra-stretchable and skin-mountable strain sensors using carbon nanotubes-Ecoflex nanocomposites. *Nanotechnology* **26**, 375501 (2015).
12. Yamada, T. et al. A stretchable carbon nanotube strain sensor for human-motion detection. *Nat. Nanotechnol.* **6**, 296–301 (2011).
13. Wang, T., Wang, R., Cheng, Y. & Sun, J. Quasi in situ polymerization to fabricate copper nanowire-based stretchable conductor and its applications. *ACS Appl. Mater. Interfaces* **8**, 9297–9304 (2016).
14. Gong, S. et al. Tattoolike polyaniline microparticle-doped gold nanowire patches as highly durable wearable sensors. *ACS Appl. Mater. Interfaces* **7**, 19700–19708 (2015).
15. Gong, S. et al. Highly stretchy black gold E-skin nanopatches as highly sensitive wearable biomedical sensors. *Adv. Electron. Mater.* **1**, 1400063 (2015).
16. Boland, C. S. et al. Sensitive, high-strain, high-rate bodily motion sensors based on graphene-rubber composites. *ACS Nano* **8**, 11 (2014).
17. Yan, C. et al. Highly stretchable piezoresistive graphene-nanocellulose nanopaper for strain sensors. *Adv. Mater.* **26**, 2022–2027 (2014).
18. Jeong, Y. R. et al. Highly stretchable and sensitive strain sensors using fragmentized graphene foam. *Adv. Funct. Mater.* **25**, 4228–4236 (2015).
19. Mattmann, C., Clemens, F. & Troster, G. Sensor for measuring strain in textile. *Sensors (Basel)* **8**, 3719–3732 (2008).
20. Kong, J.-H., Jang, N.-S., Kim, S.-H. & Kim, J.-M. Simple and rapid micropatterning of conductive carbon composites and its application to elastic strain sensors. *Carbon* **77**, 199–207 (2014).
21. Li, Q. et al. Wide-range strain sensors based on highly transparent and supremely stretchable graphene/Ag-nanowires hybrid structures. *Small* **12**, 5058–5065 (2016).
22. Zhang, H. et al. Piezoresistive sensor with high elasticity based on 3D hybrid network of sponge@CNTs@Ag NPs. *ACS Appl. Mater. Interfaces* **8**, 22374–22381 (2016).
23. Amjadi, M., Pichitpajongkit, A., Lee, S., Ryu, S. & Park, I. Highly stretchable and sensitive strain sensor based on silver nanowire–elastomer nanocomposite. *ACS Nano* **8**, 9 (2014).
24. Zhang, S. et al. Fully printed silver-nanoparticle-based strain gauges with record high sensitivity. *Adv. Electron. Mater.* **3**, 1700067 (2017).
25. Park, B. et al. Dramatically enhanced mechanosensitivity and signal-to-noise ratio of nanoscale crack-based sensors: effect of crack depth. *Adv. Mater.* **28**, 8130–8137 (2016).
26. Yang, T. et al. Structural engineering of gold thin films with channel cracks for ultrasensitive strain sensing. *Mater. Horiz.* **3**, 248–255 (2016).
27. Kang, D. et al. Ultrasensitive mechanical crack-based sensor inspired by the spider sensory system. *Nature* **516**, 222–226 (2014).
28. Choi, D. Y. et al. Highly stretchable, hysteresis-free ionic liquid-based strain sensor for precise human motion monitoring. *ACS Appl. Mater. Interfaces* **9**, 1770–1780 (2017).
29. Wang, C. et al. Carbonized silk fabric for ultrastretchable, highly sensitive, and wearable strain sensors. *Adv. Mater.* **28**, 6640–6648 (2016).
30. Ge, J. et al. A stretchable electronic fabric artificial skin with pressure-, lateral strain-, and flexion-sensitive properties. *Adv. Mater.* **28**, 722–728 (2016).
31. Kim, K. K. et al. Highly sensitive and stretchable multidimensional strain sensor with prestrained anisotropic metal nanowire percolation networks. *Nano Lett.* **15**, 5240–5247 (2015).
32. Muth, J. T. et al. Embedded 3D printing of strain sensors within highly stretchable elastomers. *Adv. Mater.* **26**, 6307–6312 (2014).
33. Rahimi, R., Ochoa, M., Yu, W. & Ziaie, B. Highly stretchable and sensitive unidirectional strain sensor via laser carbonization. *ACS Appl. Mater. Interfaces* **7**, 4463–4470 (2015).
34. Yao, S. & Zhu, Y. Nanomaterial-enabled stretchable conductors: strategies, materials and devices. *Adv. Mater.* **27**, 1480–1511 (2015).
35. Lu, N., Lu, C., Yang, S. & Rogers, J. Highly sensitive skin-mountable strain gauges based entirely on elastomers. *Adv. Funct. Mater.* **22**, 4044–4050 (2012).
36. Hwang, B. U. et al. Transparent stretchable self-powered patchable sensor platform with ultrasensitive recognition of human activities. *ACS Nano* **9**, 9 (2015).
37. Liu, Q., Chen, J., Li, Y. & Shi, G. High-performance strain sensors with fish-scale-like graphene-sensing layers for full-range detection of human motions. *ACS Nano* **10**, 7901–7906 (2016).
38. Ding, S. et al. One-step fabrication of stretchable copper nanowire conductors by a fast photonic sintering technique and its application in wearable devices. *ACS Appl. Mater. Interfaces* **8**, 6190–6199 (2016).
39. Xu, F. & Zhu, Y. Highly conductive and stretchable silver nanowire conductors. *Adv. Mater.* **24**, 5117–5122 (2012).
40. Liu, Y. L. et al. Stretchable electrochemical sensor for real-time monitoring of cells and tissues. *Angew. Chem. Int. Ed.* **55**, 4537–4541 (2016).
41. De Vivo, B. et al. Simulation and experimental characterization of polymer/carbon nanotubes composites for strain sensor applications. *J. Appl. Phys.* **116**, 054307 (2014).
42. Matsuzaki, R. & Tabayashi, K. Highly stretchable, global, and distributed local strain sensing line using GaInSn electrodes for wearable electronics. *Adv. Funct. Mater.* **25**, 3806–3813 (2015).
43. Jidong, S. et al. Graphene reinforced carbon nanotube networks for wearable strain sensors. *Adv. Funct. Mater.* **26**, 2078–2084 (2016).
44. Zhu, Y. & Xu, F. Buckling of aligned carbon nanotubes as stretchable conductors: a new manufacturing strategy. *Adv. Mater.* **24**, 1073–1077 (2012).
45. Pang, C. et al. Highly skin-conformal microhairy sensor for pulse signal amplification. *Adv. Mater.* **27**, 634–640 (2015).
46. Kim, J. et al. Stretchable silicon nanoribbon electronics for skin prosthesis. *Nat. Commun.* **5**, 5747 (2014).
47. Zhong, Z. et al. Roll-to-roll-compatible, flexible, transparent electrodes based on self-nanoembedded Cu nanowires using intense pulsed light irradiation. *Nanoscale* **8**, 8995–9003 (2016).